Available online at www.sciencedirect.com

ScienceDirect

Procedia Manufacturing 38 (2019) 1189–1196

Procedia MANUFACTURING

www.elsevier.com/locate/procedia

29th International Conference on Flexible Automation and Intelligent Manufacturing (FAIM2019), June 24-28, 2019, Limerick, Ireland.

Comparative evaluation of adhesively-bonded single-lap and stepped-lap joints

J.O.S. Silva[a], R.D.S.G. Campilho[a,b,*], R.J.B. Rocha[a,b], F.J.G. Silva[a]

[a]*ISEP-School of Engineering, Rua Dr. António Bernardino de Almeida 431, 4200-072 Porto, Portugal*
[b]*INEGI, Campus da FEUP, Rua Dr. Roberto Frias 400, 4200-465 Porto, Portugal*

Abstract

Several adhesive joint configurations are available, namely butt joints, single-lap joints (SLJ), double-lap joints and scarf joints. Stepped-lap joints, which are not so studied, consist of a finite number of steps in the bonded area, possessing stress concentrations at all step edges instead of only at the bonded length edges. Stepped-lap joints increase the maximum load (P_m) over SLJ. The present study experimentally and numerically evaluates the static tensile strength of SLJ and stepped-lap joints bonded with the moderately ductile adhesive Araldite® 2015, considering varying values of overlap length (L_O). A Finite Element Method (FEM) analysis was carried out to compare through-thickness normal (σ_y) and shear (τ_{xy}) stresses in the bondline between joint configurations. Additionally, a Cohesive Zone Modelling (CZM) analysis was considered to study the failure modes and to evaluate the CZM technique's accuracy. Between SLJ and stepped-lap joints, the improved stress distributions of the stepped-lap joints resulted in higher joint performance, especially for higher L_O. The CZM model revealed to be accurate in predicting P_m.

Keywords: Adhesive joints; Stepped-lap joint; Finite Element Analysis; Cohesive Zone Models; Stress analysis.

* Corresponding author. Tel.: +351-939526892; fax: +351-228321159.
E-mail address: raulcampilho@gmail.com

10.1016/j.promfg.2020.01.209

1. Introduction

Adhesive bonding is currently a widespread joining method in several industrial fields (e.g. aerospace, automotive, naval, wind energy, construction, furniture and footwear) [1], presenting a number of benefits compared to other methods, e.g. riveted, bolted or welded joints [2]. In fact, one of its great advantages is the ability of obtain lightweight and stronger structures. In addition, adhesive bonding provides more uniform stress distributions than the other methods, better aesthetics, lower manufacturing costs and the possibility to join dissimilar materials. Irrespectively of these, drawbacks include the need of surface preparation, typical disassembly by inducing damage in the structures, and joint design orientated towards the elimination of σ_y stresses [3]. Several joint configurations are available for the designer, namely butt joints, SLJ, double-lap joints and scarf joints [4]. In addition, stepped-lap joints, which are not so studied as the others, consist of a finite number of steps in the bonded area, possessing stress concentrations at all step edges instead of only at the bonded length edges [5]. Stepped-lap joints promote a noteworthy increase in P_m over SLJ. Indeed, the former can attain higher P_m due to the gradual load transfer from step to step [6].

An accurate prediction of the joints behavior is required for a widespread use of this bonding technology. The strength prediction of bonded joints began about eighty years ago with analytical techniques by Volkersen [7]. Through these techniques, bonded joints were quickly evaluated. Nevertheless, the forthcoming of novel and complex adhesives with large plasticity gives rise to a higher complexity of the analysis, leading to the progressive use and improvement of numerical methods. A nowadays widespread method that was initially purposed by Barenblatt [8, 9] and Dugdale [10], is CZM. Subsequently, this technique was improved and implemented in FEM software in order to simulate the fracture behavior. CZM is based on cohesive elements [11], and on the establishment of traction-separation laws connecting solid elements. The most commonly used are the triangular laws [12], although more refined models are available, such as exponential [13] or trapezoidal [14]. In recent times, the eXtended Finite Element Method (XFEM) has been applied to the crack propagation simulation [15], including bonded joints [16].

Compared with other joints architectures, a small number of works evaluates stepped-lap joints, on metallic or composite adherends. Akpinar [5] studied three joint designs, namely SLJ, one stepped-lap and three stepped-lap joints, bonding aluminum with two adhesives of different ductility grades. The joint width (B), adhesive thickness (t_A) and L_O were kept identical between the three joints. The author found that the joint architecture significantly affects the stress concentrations in the bondline and P_m. In fact, it was concluded that the steps enable the decrease of σ_y peak stresses at the overlap edges. On the other hand, evaluating P_m of the different designs, the flexible adhesive showed an increase of 11% for the one stepped-lap joint and 60% for the three stepped-lap joint, when compared with the SLJ. For the stiff adhesive, these differences were of 9% and 68%, respectively. Bendemra et al. [17] evaluated the effect of the ply thickness, t_A, stacking sequence, over ply layup, and over ply lap length on σ_y and τ_{xy} peak stresses in the bondline of scarf and stepped-lap bonded repairs. The outcomes showed that, for both repair procedures, increasing the ply thickness from 0.13 to 0.39 mm decreased the peak stresses. In fact, normalized σ_y peak stresses were reduced by 81 and 53% in the scarf and stepped-lap joints, respectively. τ_{xy} peak stresses were also affected by -77 and 54%, in the same order. By increasing t_A from 0.13 to 0.39 mm, a significant increase in σ_y and τ_{xy} peak stresses, of approximately 170%, occurred for the tapered scarf repairs. On the other hand, for the stepped-lap repairs, the same t_A variation led to an increase of 26% in σ_y peak stresses and a decrease of 10% in τ_{xy} peak stresses. Despite the stepped-lap repairs possess higher stress concentration than equivalent scarf repairs, the introduction of over plies and modifications in the joint design is prone to reduce peak stresses.

The present study experimentally and numerically evaluates the static tensile strength of SLJ and stepped-lap joints bonded with the moderately ductile adhesive Araldite® 2015, considering varying values of L_O. A FEM analysis was carried out to compare σ_y and τ_{xy} stresses in the bondline between joint configurations. Additionally, a CZM analysis was considered to study the failure modes and to evaluate the CZM technique's accuracy.

2. Experimental work

2.1. Adhesives and adherends characterization

The AW6082 T651 high strength aluminum alloy was selected as the adherend material. The stress-strain (σ-ε) curves of this material were obtained as described in the standard ASTM-E8M-04 [18]. The evaluated mechanical

properties are as follows: Young's modulus (E) of 70.07±0.83 GPa, tensile yield stress (σ_e) of 261.67±7.65 MPa, tensile strength (σ_f) of 324.00±0.16 MPa and tensile failure strain (ε_f) of 21.70±4.24% [12]. The ductile epoxy adhesive Araldite® 2015, evaluated in this work, was previously characterized regarding the required mechanical and fracture properties [12, 14]. The mechanical properties in tension (E, σ_e, σ_f and ε_f) were found by bulk dogbone specimens, fabricated as specified in the Standard NF T 76-142. Fig. 1 depicts an example σ-ε curve of the adhesive Araldite® 2015.

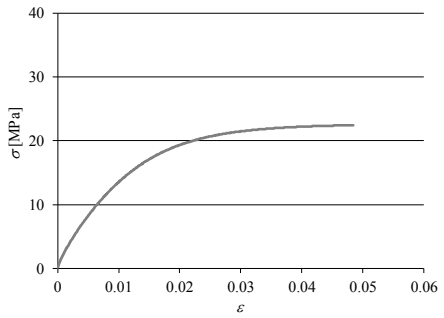

Fig. 1 –Example σ-ε curve of the Araldite® 2015

Furthermore, thick adherend shear tests (TAST) were performed to estimate the shear mechanical properties. σ_e and the shear yield stress (τ_e) were calculated for a plastic strain of 0.2% in the respective curves. The tensile toughness (G_{IC}) and shear toughness (G_{IIC}) estimation was accomplished by Double-Cantilever Beam (DCB) and End-Notched Flexure (ENF) tests, respectively, using robust data reduction schemes. Details of the fabrication process of these specimens can be found in a former work [19]. The obtained properties are presented in Table 1.

Table 1 – Mechanical and fracture properties of the adhesive Araldite® 2015 [12, 14]

Property	**2015**
Young's modulus, E [GPa]	1.85±0.21
Poisson's ratio, ν	0.33 [a]
Tensile yield stress, σ_e [MPa]	12.63±0.61
Tensile strength, σ_f [MPa]	21.63±1.61
Tensile failure strain, ε_f [%]	4.77±0.15
Shear modulus, G [GPa]	0.56±0.21
Shear yield stress, τ_e [MPa]	14.6±1.3
Shear strength, τ_f [MPa]	17.9±1.8
Shear failure strain, γ_f [%]	43.9±3.4
Toughness in tension, G_{IC} [N/mm]	0.43±0.02
Toughness in shear, G_{IIC} [N/mm]	4.70±0.34

[a] manufacturer's data
[b] estimated in reference [12]

2.2. Joint dimensions and manufacturing procedures

Fig. 2 describes the generic geometry and parameters of the SLJ (a) and stepped-lap joints (b).

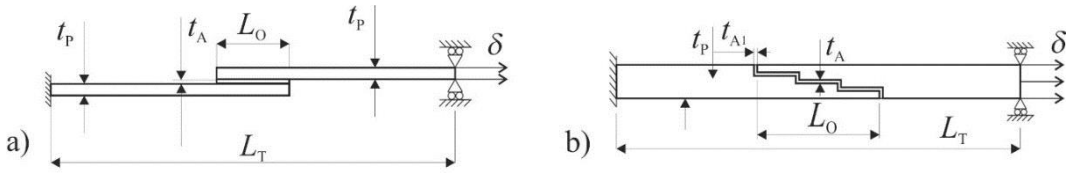

Fig. 2 – SLJ (a) and stepped-lap joints (b) geometry

Regarding the SLJ, the dimensions of the specimens are: joint length between grips L_T=170 mm, adherends' thickness t_P=3 mm, B=25 mm, t_A=0.2 mm and L_O=12.5, 25, 37.5 and 50 mm. In all stepped-lap joint configurations, the bonded length was divided into three steps of equal length, and an identical step height increment was applied in consecutive steps. The geometric parameters were: L_T=180 mm, t_P=3 mm, B=25 mm, t_A=0.2 mm, adhesive thickness of the vertical portions t_{A1}=0.2 mm and L_O=12.5, 25, 37.5 and 50 mm. Five joints were fabricated and tested for each configuration and joint design, defined by L_O, making up a total of 20 SLJ and 20 stepped-lap joints. The joints manufacturing process started by cutting the supplied plate to the final width (B=25 mm) and length. For the stepped-lap joints, milling of the steps in a vertical mill was required as well. Before applying the adhesive, the bonding surfaces were grit-blasted with corundum sand to remove the surface oxide layer and contaminants, and then cleaned with acetone and allowed to dry before application of the adhesive. After, the adhesive was poured in the bonding surfaces and the joints were assembled. With this purpose, the adherends were fixed in an apparatus for the correct alignment. A calibrated wire with a diameter of 0.2 mm was placed under the upper adherend to ensure a constant t_A. For the SLJ, tabs were glued at the specimens' edges to ensure a correct alignment in the testing machine. This was not required for the stepped-lap joints. The joints were left to cure at room temperature for one week to assure complete curing. To provide square edges at the overlap, the excess adhesive was removed using a grindstone in a vertical drill. Both SLJ and stepped-lap joints were tested in a Shimadzu AG-X 100 equipment using a load cell of 100 kN, at room temperature and with a testing speed of 1 mm/min. For each joint type, a minimum of four valid results was guaranteed.

3. Numerical simulations

The numerical evaluation was carried out in Abaqus® considering two-dimensional (2D) models under plane-strain assumptions. The analysis was geometrical non-linear to accurately account for transverse deflections [20]. The adherends were modelled as isotropic with plasticity [21]. On the other hand, the adhesive layer was treated either using elastic solid elements (for the stress analysis) or with cohesive elements (for the failure analysis). The SLJ were modelled by a single layer of CZM elements, while the stepped-lap joints were modelled by horizontal and vertical segments of CZM elements, leaving a small gap between them. Fig. 3 shows a mesh detail at the overlap for the stepped-lap joints with L_O=12.5 mm. For the failure analysis, CZM elements of dimensions 0.2×0.2 mm^2 were used. Oppositely, the mesh density is much more refined for the stress analysis, since ten elements were used through-thickness in the adhesive, in order to achieve the desired accuracy. As boundary conditions, the joints were clamped at one edge and loaded by a tensile displacement while vertical restrained at the opposing edge [22, 23]. The next Section gives details on the mixed-mode triangular CZM implemented in Abaqus®, which was used in this work.

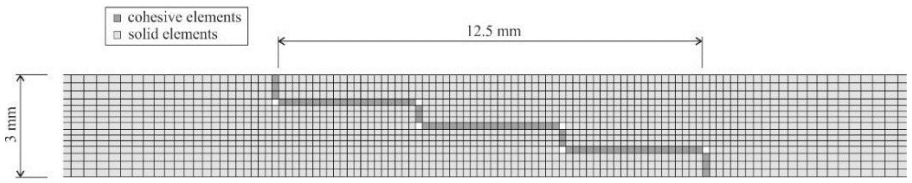

Fig. 3 – Mesh for a stepped-lap joint with L_O=12.5 mm

3.1. Triangular CZM theory

Relationships among stresses and relative displacements linking similar nodes of cohesive elements are the fundament of the CZM. Additionally, those relations (often entitled CZM laws) may be established in pure and mixed mode and make possible to capture the material's behavior up to failure [24]. This study relies on triangular pure and mixed-mode laws to model the adhesive layer (Fig. 4).

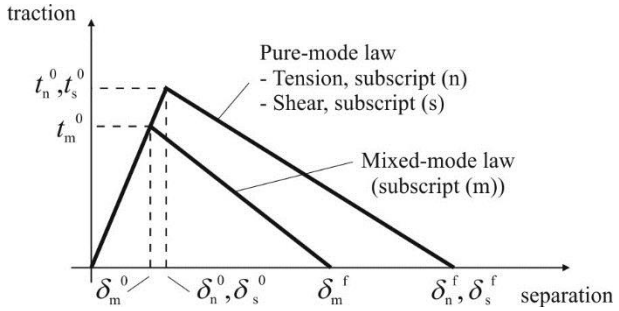

Fig. 4 – Mixed-mode triangular CZM law used in Abaqus® [25]

Under pure-mode loading, damage initiation occurs when the cohesive strength in tension or shear (t_n^0 or t_s^0, respectively) is attained, i.e., the material's elastic behavior is cancelled and degradation starts [26]. Furthermore, the crack propagates up to the adjacent pair of nodes when the values of current tensile or shear cohesive stresses (t_n or t_s, respectively) become null. Under mixed-mode loading, stress and/or energetic criteria are often used to combine the pure-mode laws, and damage begins when the mixed mode cohesive strength (t_m^0) is reached [27]. Several criteria are available for damage initiation and growth when the analysis encompasses mixed-mode loadings. Nevertheless, this study focused on the quadratic nominal stress criterion and a linear power law form for the damage initiation and growth, respectively. This model is described in detail in the work of Rocha and Campilho [22]. The adhesives' properties used in Abaqus® are depicted in Table 2 (properties derived from the information of Table 1).

Table 2 – Cohesive properties for the adhesive Araldite® 2015

E [GPa]	1.85	t_s^0 [MPa]	17.9
G [GPa]	0.56	G_{IC} [N/mm]	0.43
t_n^0 [MPa]	21.63	G_{IIC} [N/mm]	4.70

4. Results

4.1. σ_y and τ_{xy} stresses

σ_y and τ_{xy} stresses were analyzed at the middle of the adhesive layer and plotted as a function of x/L_O ($0 \leq x \leq L_O$ between both overlap edges). Both were divided by τ_{avg}, the average τ_{xy} for the respective L_O, and they relate to the stage where the adherends and adhesive are in the elastic domain. Fig. 5 shows the σ_y (a) and τ_{xy} (b) stress distributions for the SLJ and stepped-lap joints bonded with the Araldite® 2015 for L_O=12.5 and 50 mm.

Regarding σ_y stresses and L_O=12.5 mm, it is notorious that the SLJ has the highest peak stresses (σ_y/τ_{avg} of 3.19). Actually, the stepped-lap joint presents smaller σ_y peak stresses by -76.1% for L_O=12.5 mm, when compared to the SLJ. This behavior is due to the load asymmetry, leading to significant joint rotations and corresponding σ_y peak stresses at the overlap edges [2]. By increasing L_O, a degradation of stress distributions occurs, leading to the increase of stress gradients. In fact, an increase of 170.4 and 206.7% was found by increasing L_O from 12.5 to 50 mm for SLJ and stepped-lap joint, respectively. Nevertheless, oppositely to the SLJ, the stepped-lap joint has the capability to distribute the stresses by the steps, which is reflected in the difference found for x/L_O=0 and 1. Actually, the stepped-lap joints present σ_y stress deviations of -72.3% for L_O=50 mm, when comparing to the SLJ. Compressive σ_y peak stresses at the two inner step transitions ($x/L_O \approx 0.33$ and 0.67) were found for the stepped-lap joints. Despite the step-induced stress variations, the behavior is similar to the SLJ [28, 29], and is caused by the adherends' rotation that promotes peeling of the overlap edges and compresses the region in-between.

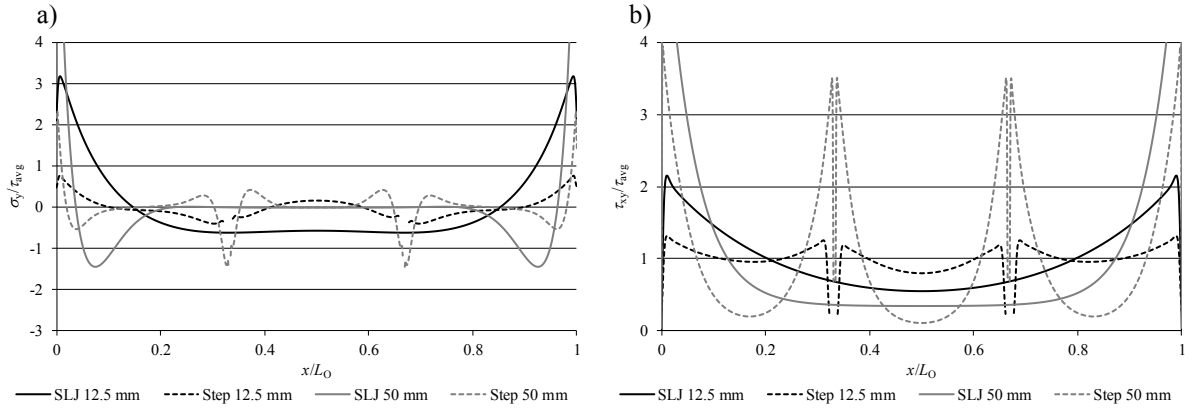

Fig. 5 – σ_y (a) and τ_{xy} (b) stress distributions for the SLJ and stepped-lap joints for L_O=12.5 and 50 mm

The τ_{xy} stress distributions depicted in Fig. 5 (b) show, for L_O=12.5 mm, that the τ_{xy} peak stresses are higher for the SLJ by 39.3%, compared to the stepped-lap joint. Actually, the SLJ plot deviates the most from τ_{avg}, reaching a maximum τ_{xy}/τ_{avg} of 2.2. This behavior is justified from the significant shear-lag or differential deformation effect of the adherends [28]. The step design and thickness reduction in the direction of the adherends ends at the overlap are capable to distribute the loading in a much more efficient manner between the steps [17]. By comparing different L_O, it is evident that τ_{xy} peak stresses increase with this parameter for both joint designs. This happens because of the increasing gradients of adherends' axial deformation within each step for higher L_O for the stepped-lap and increase of differential deformation of the two adherends at the overlap for the SLJ. For the SLJ with L_O=50 mm, τ_{xy} peak stresses deviate 196.5% compared to L_O=12.5 mm. As for the stepped-lap joint, τ_{xy} peak stresses increase 201.8% by increasing L_O. Thus, this discussion makes clear that the stepped-lap joint should perform best for the same bonded area of adhesive, compared to the SLJ.

4.2. Failure modes

Generally, the experimental tensile tests showed a cohesive failure of the adhesive for both joint architectures. Regarding the SLJ, damage initiation occurs at the overlap edges and grows towards the center until the load becomes higher than the strength of the adhesive. Minor adherends' plasticization was found for L_O=50 mm. For the stepped-lap joints, adherends' plasticization was found from L_O=37.5 mm. Moreover, for L_O=50 mm, few specimens failed by adherends' net failure, due to the higher loads and smaller cross section. This type of failure stands for an efficient bonding. During the experiments, the failure paths of the stepped-lap joints were not possible to capture. On the other hand, the numerical simulations provided a full perspective of the joints' behavior during the failure phase. Fig. 6 presents the damage locations' nomenclature for the stepped-lap joints. For $12.5 \leq L_O \leq 37.5$ mm, the damage path was similar. Damage started at the vertical outer steps transitions (1) followed by the middle sections (2), which is in accordance with the previous stress analysis, which indicated these regions as highest stressed. Damage then grew to the outer steps (3), finishing in the middle step (4). For L_O=50 mm, the first two stages were identical. Then, either cohesive failure of the adhesive at (3) and (4), or by the adherend, took place.

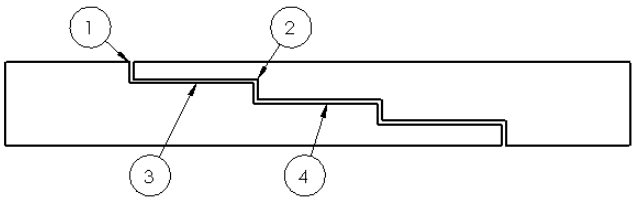

Fig. 6 – Numerical failure locations in the stepped-lap joints

4.3. SLJ and stepped-lap joint P_m comparison

Fig. 7 compares the experimental and numerical P_m of the SLJ and stepped-lap joints as a function of L_O. The P_m evaluation that follows takes into account the previous stress analysis. Both joint designs attained identical experimental P_m for L_O=12.5 mm: 5.3 kN and 5.2 kN found for the SLJ and stepped-lap joint, respectively. Moreover, the numerical predictions were very accurate, with deviations by -0.9 and -2.3%, in the same order. For short overlaps, σ_y and τ_{xy} stresses are typically more uniform regardless the joint type, as it can be attested in Fig. 5. Under these conditions, an adhesive that has a moderate ductility, such as the Araldite® 2015, manages to absorb peak stresses, and no significant variations arising from the improved stress distributions of the stepped-lap joints over the SLJ. By increasing L_O to 25 mm, the joints' strength was largely improved. Actually, increases of 79.3 and 101.3% were found for the SLJ and stepped-lap joint, respectively. Once more, good numerical results were obtained, with deviations of -0.8% (SLJ) and 0.4% (stepped-lap). Here, a non-negligible P_m difference exists between both joint types, with advantage to the stepped-lap joints. Increasing L_O brings higher peak stresses (Fig. 5), more significant for the SLJ which, coupled with the limited ductility of the adhesive, now translates into a smaller P_m improvement for this joint. On the other hand, by further increasing L_O to 37.5 mm, improvements were lower than with the previous L_O increment. Compared to L_O=25 mm, the P_m improvements were only 29.1 and 38.8% for the SLJ and stepped-lap joints, respectively. The numerical simulations were able to capture this behavior with deviations from the experimental values of 5.7 and 2.4%, in the same order of joint type. The previously discussed trend, with smaller P_m performance for the SLJ, continues to occur, and the overall P_m different between consecutive L_O further decreases because, although the stepped-lap joints excel SLJ in the stress distributions, its peak stresses increase as well. The smallest P_m variations were those between L_O=37.5 and 50 mm, corresponding to 24.1% (SLJ) and 17.3% (stepped-lap). The numerical outcomes were once again accurate, presenting deviations from of the experiments of 5.9 and 2.0% (in the same order). For this L_O, peak stresses are highest (Fig. 5), and this results in the smallest P_m improvement. Between limit L_O (12.5 and 50 mm), the overall P_m increase was 187.1% (SLJ) and 227.6% (stepped-lap joint). The maximum relative improvement of stepped-lap joints over SLJ (for L_O=50 mm) was 13.1% (considering the experimental P_m values).

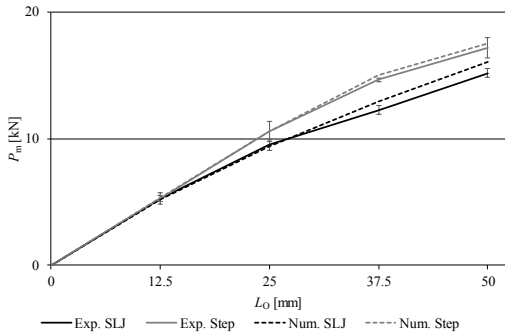

Fig. 7 – Experimental results and CZM predictions of P_m as a function of L_O for the Araldite® 2015

5. Conclusions

The present work aimed at performing an experimental and numerical (CZM) comparison between tensile-loaded SLJ and stepped-lap joints, bonded with a moderately ductile adhesive (Araldite® 2015), as a function of L_O. An initial σ_y and τ_{xy} stress analysis revealed different stress fields between joint types, with higher magnitude peaks for the SLJ. This behavior could be attributed to the lack of load-collinearity and higher shear-lag effects in the SLJ, which reflected on bigger stress gradients, typically at the overlap edges. Moreover, σ_y stresses were typically smaller than τ_{xy} for both joint types, except at the overlap edges for some conditions. Both SLJ and stepped-lap joints experienced a significant increase of peak stresses for higher L_O. The P_m comparison revealed accurate strength predictions overall, and a monotonic P_m increase with L_O, although at a decreasing rate with L_O, which agrees with the previous stress

analysis results. Between joint types, for short L_O, the two joint types gave similar P_m results since, by using a moderately ductile adhesive, it can still absorb peak stresses if these are not too significant. However, as L_O increases, the adhesive partially loses this ability, which then translates into a growing difference between the SLJ and stepped-lap joints, with advantage to the latter because of the improved stress distributions. As a final conclusion in the performance comparison, stepped-lap joints may benefit from a flush joining region without adherends' eccentricity and provide a better performance than SLJ. In the present study, the maximum difference was 13.1%, for L_O=50 mm, and with tendency to increase if higher L_O were considered. However, this has to be weighed against the ease of fabrication and absence of machining of SLJ for the final selection of the best joint configuration for a given application.

References

[1] R.D. Adams. Adhesive bonding: science, technology and applications. Cambridge: Woodhead Publishing Limited; 2005.
[2] E.M. Petrie. Handbook of adhesives and sealants. New York: McGraw-Hill; 2000.
[3] Ö. Öz, H. Özer, An experimental investigation on the failure loads of the mono and bi-adhesive joints, Journal of Adhesion Science and Technology, 31 (2017) 2251-70.
[4] S. Murakami, Y. Sekiguchi, C. Sato, E. Yokoi, T. Furusawa, Strength of cylindrical butt joints bonded with epoxy adhesives under combined static or high-rate loading, International Journal of Adhesion and Adhesives, 67 (2016) 86-93.
[5] S. Akpinar, The strength of the adhesively bonded step-lap joints for different step numbers, Composites Part B: Engineering, 67 (2014) 170-8.
[6] R.D. Adams, J. Comyn, W.C. Wake. Structural adhesive joints in engineering. 2nd ed. London: Chapman & Hall; 1997.
[7] O. Volkersen, Die Niektraftverteilung in zugbeanspruchten mit konstanten laschenquerschritten, Luftfahrtforschung, 15 (1938) 41-7.
[8] G.I. Barenblatt, The formation of equilibrium cracks during brittle fracture. General ideas and hypothesis. Axisymmetrical cracks., Journal of Applied Mathematics and Mechanics, 23 (1959) 622-36.
[9] G.I. Barenblatt, The Mathematical Theory of Equilibrium Cracks in Brittle Fracture, Advances in Applied Mechanics, 7 (1962) 55-129.
[10] D.S. Dugdale, Yielding of steel sheets containing slits, Journal of the Mechanics and Physics of Solids, 8 (1960) 100-4.
[11] P. Feraren, H.M. Jensen, Cohesive zone modelling of interface fracture near flaws in adhesive joints, Engineering Fracture Mechanics, 71 (2004) 2125-42.
[12] R.D.S.G. Campilho, M.D. Banea, A.M.G. Pinto, L.F.M. da Silva, A.M.P. de Jesus, Strength prediction of single- and double-lap joints by standard and extended finite element modelling, International Journal of Adhesion and Adhesives, 31 (2011) 363-72.
[13] M. Malekan, Finite element simulation of gaseous detonation-driven fracture in thin aluminum tube using cohesive element, Journal of the Brazilian Society of Mechanical Sciences and Engineering, 38 (2016) 989-97.
[14] R.D.S.G. Campilho, M.D. Banea, J.A.B.P. Neto, L.F.M. da Silva, Modelling adhesive joints with cohesive zone models: effect of the cohesive law shape of the adhesive layer, International Journal of Adhesion and Adhesives, 44 (2013) 48-56.
[15] G. Liu, D. Zhou, J. Ma, Z. Han, Numerical investigation of mixed-mode crack growth in ductile material using elastic–plastic XFEM, Journal of the Brazilian Society of Mechanical Sciences and Engineering, 38 (2016) 1689-99.
[16] A. Mubashar, I.A. Ashcroft, A.D. Crocombe, Modelling damage and failure in adhesive joints using a combined XFEM-cohesive element methodology, The Journal of Adhesion, 90 (2014) 682-97.
[17] H. Bendemra, P. Compston, P.J. Crothers, Optimisation study of tapered scarf and stepped-lap joints in composite repair patches, Composite Structures, 130 (2015) 1-8.
[18] ASTM-E8M-04. Standard test methods for tension testing of metallic materials [Metric]. West Conshohocken, PA: ASTM International; 2004.
[19] A.C.C. Leitão, R.D.S.G. Campilho, D.C. Moura, Shear Characterization of Adhesive Layers by Advanced Optical Techniques, Experimental Mechanics, 56 (2016) 493-506.
[20] P.C. Pandey, S. Narasimhan, Three-dimensional nonlinear analysis of adhesively bonded lap joints considering viscoplasticity in adhesives, Computers & Structures, 79 (2001) 769-83.
[21] S.L.S. Nunes, R.D.S.G. Campilho, F.J.G. da Silva, C.C.R.G. de Sousa, T.A.B. Fernandes, M.D. Banea, et al., Comparative failure assessment of single and double-lap joints with varying adhesive systems, The Journal of Adhesion, 92 (2016) 610-34.
[22] R.J.B. Rocha, R.D.S.G. Campilho, Evaluation of different modelling conditions in the cohesive zone analysis of single-lap bonded joints, The Journal of Adhesion, (2017) in press.
[23] R.D.S.G. Campilho, T.A.B. Fernandes, Comparative Evaluation of Single-lap Joints Bonded with Different Adhesives by Cohesive Zone Modelling, Procedia Engineering, 114 (2015) 102-9.
[24] H. Luo, Y. Yan, T. Zhang, Z. Liang, Progressive failure and experimental study of adhesively bonded composite single-lap joints subjected to axial tensile loads, Journal of Adhesion Science and Technology, 30 (2016) 894-914.
[25] Abaqus®. Documentation of the software Abaqus®. Dassault Systèmes. Vélizy-Villacoublay 2013.
[26] A.U. Sane, P.M. Padole, C.M. Manjunatha, R.V. Uddanwadiker, P. Jhunjhunwala, Mixed mode cohesive zone modelling and analysis of adhesively bonded composite T-joint under pull-out load, Journal of the Brazilian Society of Mechanical Sciences and Engineering, 40 (2018) 167.
[27] R. Dimitri, M. Trullo, L. De Lorenzis, G. Zavarise, Coupled cohesive zone models for mixed-mode fracture: A comparative study, Engineering Fracture Mechanics, 148 (2015) 145-79.
[28] B. Zhao, Z.-H. Lu, Y.-N. Lu, Two-dimensional analytical solution of elastic stresses for balanced single-lap joints—Variational method, International Journal of Adhesion and Adhesives, 49 (2014) 115-26.
[29] M. Goland, E. Reissner, The stresses in cemented joints, Journal of Applied Mechanics, 66 (1944) A17–A27.